Determination of effective hole mass in $Hg_{1-X}Cd_XTe$ by ARPES

Matthias Kreier
Institut für Physik, Humboldt Universität zu Berlin
matthias.kreier@physik.hu-berlin.de

Abstract

Several samples of $Hg_{1-X}Cd_XTe$ with X values between 0.07 and 0.4 were investigated by ARPES. Because this method is very surface sensitive, we will also consider surface problems and requirements. Using the methods of Laue, LEED, SEM and AFM we checked the surfaces that were preparated by cleaving. Based on a proven good surface quality we represent our photo emission spectra in normal emission, taken at BESSY at photon energies between 44 and 125 eV. Thereafter the fitted spectra were assigned to the representing points inside the Brillouin zone. Concludingly we can directly fit the dispersion and derive the effective hole mass of different bands as well as the energy separation by the spin-orbit interaction. These results are compared to already well known effective mass values

1 Introduction

The method of Angle Resolved Photo Electron Spectroscopy (APRES) is a unique method to observe the bandstructure of a sample. With this technique it is possible to compare directly the theoretically calculated bandstructure with the real states of electrons inside a material. Other methods having an indirect approach depend on the used model and the right interpretation of the results.

The following measurements were taken with the High Resolution Photo Electron Spectrometer (HIRES-PES) of the EES group of Prof. R. Manzke at the Humboldt University to Berlin. It uses a Omicron AR65 electron analyser with a achievable resolution of 10 meV. The different photon energies were supplied by the BUS-beamline at the BESSY synchrotron.

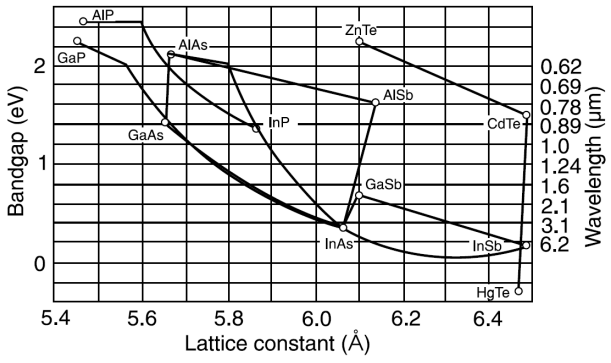

Fig. 1: Comparison of the bandgap vs. lattice constant variation with the lattice constant for a varity of III-V compounds.

The samples of $Hg_{1-X}Cd_XTe$ were gradually provided by the Faculty of Low Temperature Physics and Supraconductors at the Moscow State University. Special thanks belongs to Dr. Никифоров Владимир Николаевич and Prof. В. Г. Средин.

2 Crystal Quality

In our investigation we analysed the effect of different X values in the composition of $Hg_{1-X}Cd_XTe$ to the bandstructure. CdTe is a semiconductor with 1.6 eV bandgap. HgTe is reffered to be a semimetal. More precise it is described as a zero-gap semiconductor with an inverted bandstructure. HgTe has a negative band gap of -0.34 eV. Both materials have a direct bandgap and very similar lattice constants (HgTe 6.445 Å, CdTe 6.488 Å). They can be mixed into alloys of any ratio between Cd_X and Hg_{1-X}. By varying the X value of the composition the bandgap can be adjusted to a deserved value (see figure 1, after [22]). Regarding the lattice match the alloy $Cd_{0.96}Zn_{0.04}Te$ is a good substrate for MWIR and LWIR applications.

Supplied by the Moscow institute we got a variety of alloys with different X values from 0.07 to 0.4. An overview of these six investigated samples is given in table 1. The material HgTe has already been investigated by N. Orlowski in our workgroup [19]. The respective X value would be zero.

Sample	value of X	weight	orientation
I	0.07	186.3 mg	[111]
II	0.4	130.3 mg	
III	0.2	158.5 mg	[110]
IV	0.183	129.2 mg	[110]
V	0.1955	248.5 mg	[110]
VI	0.105	108.9 mg	[110]

Table 1: Data of investigated samples

For angle resolved measurements the orientation of the samples plays a vital role. We first checked the orientation of all 6 samples by the Laue reflection method. The measurements has been done in Moscow by Телегина Инна Васильевна at the кафедре физики твёрдого тела или кафедре физики конденсированных сред. All pictures were taken at 32 kV

and 30 mA with an exposure time of 10 minutes. The film was located 40 mm from the sample. One example can be seen in figure 2.

The Laue method is also sensitive to polychrystallic parts. But on the photograph no disturbing spots of different crystal orientation can be seen. We observe clear and bright spots, which proves a good single crystal quality.

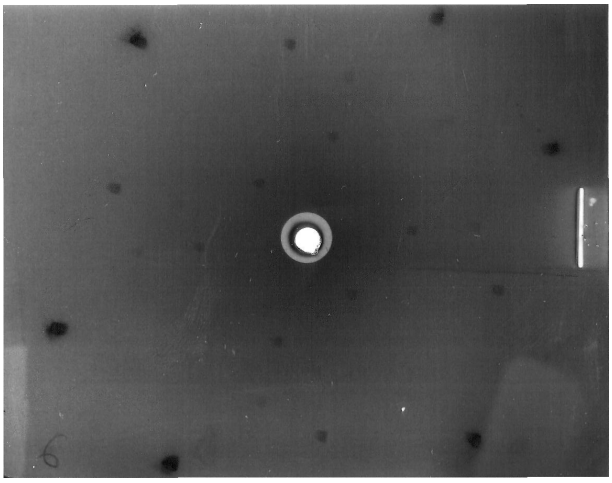

Fig. 2: Laue reflection picture of [110] surface of sample II.

The distribution of the Laue reflexes belongs to a [110] surface that is tilted by some 2 degrees. The [110] is the natural cleavage direction of ZnS crystals and the surface we investigated. It has no dangeling bonds but is electrically neutral.

Next we checked the surface using the AFM (Atomic Force Microscope) of the Moscow Biomedical Institute at Kaschirskoje. In the following picture the remaining fragments of the electro erosion saw can be seen. On the left we see a channel of 1μm width and 50nm depth. If we zoom in further we see many more parallel structures that remained from the fragmentation of the incidend big bulk crystal.

Spicer *et. al.* [8] reportet a movement of dislocation states from the bulk to the surface at roomtemperature due to the weak Hg bond. In the AFM picture they can be seen inside the channel. The parallel periodic structure are disturbed by some bumps of 10nm height and 30nm diameter.

The small valley in diagonal direction seems to be a remaining scratch from the sample preparation with tweezers. This is another sign for the fragile surface of HgCdTe and the attention it requires to work with this alloy.

3 Surface preparation

The ARPES method is only sensitive to the first few Åof the sample, but the results should represent the bulk properties. The main reason is the short mean free path of excitated electrons inside the bulk material (see figure 4) at UPS energies. Investigating a material using

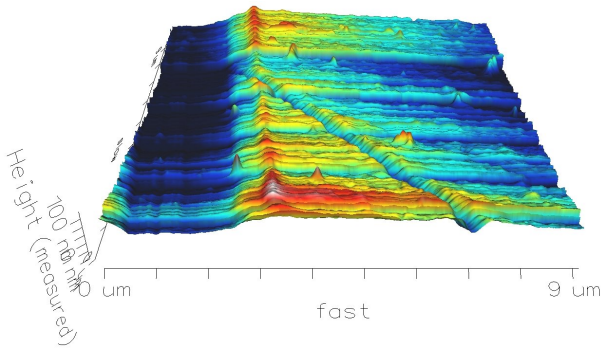

Fig. 3: This surface has been preparated mechanically by a electropyrolytic saw for dividing bigger monocrystal blocks. Thereafter the surface was cleaned chemically. One can see disslocations that moved to the surface.

this method several surface effects have to be minimized or eliminated. Therefore a clean surface plays a vital role. All measurement are taken in UHV (Ultra High Vacuum, $P < 10^{-9} mbar$) conditions. Using a simple thermodynamic approximation one can show that in this case there are several hours until adsorption or covering processes change the surface.

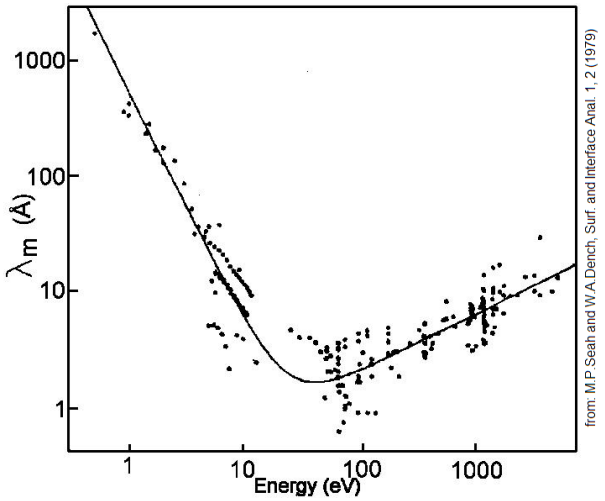

Fig. 4: Mean free path λ_m of electrons in matter, depending on kinetic energy.

A crystal transfered from normal air pressure conditions into vacuum has to be prepared before measurement. One common method for metals is the combination of sputtering and annealing. Yet this procedure does'nt apply for HgCdTe as the surface crystal structure is disturbed in a extrem way [8]. The roughtness reaches several Nanometer. The crystal structure changes and differes some hundered Nanometer from the bulk crystal structure. And even the composition changes in a dimension that can't be neglected. One reason is the high partial pressure of Hg.

Therefore we used a cleavage mechanism for surface preparation, as did other groups ([7], [10] and [11]) prior to us. For the investigation of HgTe N. Orlowski constructed a special cleavage chamber. The Moscow samples are that small and thin, that the cleavage can be

done directly inside the sample holder, using a shop glued to the top of the sample. Our group uses this method to cleave van-der-Waals crystals. For these small crystals with covalent bondings this method also applies.

Our first cleavage we performed at room temperature. The results we checked thereafter with a scanning electron microscope. Some steplike structure in the μm range can be observed. Another surface sensitive method is LEED, but we were unsuccessfull in getting a picture of the uncooled cleaved sample.

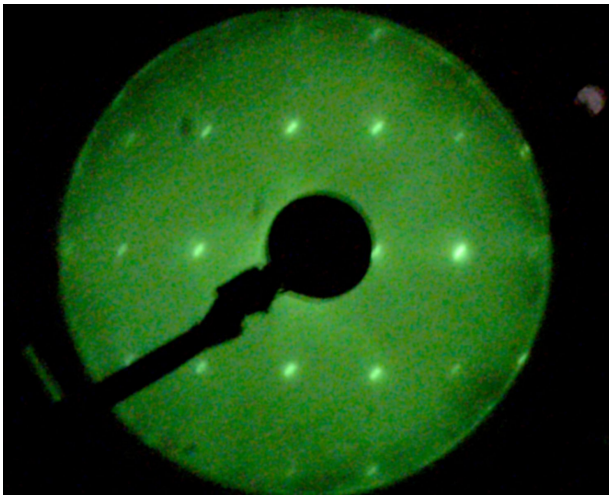

Fig. 5: Successfull LEED picture at 156 eV after cooled cleavage with liquid nitrogen.

In June 2007 finally we did a cooled cleavage inside the vacuum. The sample was mounted into a sample holder on a manipulator, that can be cooled by liquid nitrogen and helium. We used N_2^{fl} and reached a temperature of 100K at the sample. After the cleavage we were able to see the first LEED picture (see figure 5) of our sample.

From this picture one can derive the lattice constants, using the incident electron energy and geometry of the LEED analyser. With picture 5 we derived the lattice constants a=3.5 Å and b=2.4 Å , which is consistant with the [110] surface of HgCdTe.

4 ARPES spectra of HgCdTe

At photon energies usually avaliable on a Synchrotron as BESSY one gets a photo electron spectra as shown in picture 6. The core levels of Te (4d) and Hg (5d) show now dispersion and are not considered in the following. In the energy band from -6.5 to -4 eV some Hg6s states can be observed, as can be seen in figure 7. These level only reveal some intensity modulation due to matrix element effects rather than any dispersion. Therefore we will only consider the energy range of -4 to 0 eV, where zero is defined by the fermi energy.

All the following spectra were taken in normal emission. The recorded data where very noisy, so they were smoothed several times [4] using the formula

$$I_S(N) = \frac{1}{4}[I(N-1) + 2I(N) + I(N+1)] \ . \qquad (1)$$

Here we named intensity after the smoothing operation $I_S(N)$. The intensities were normalised.

Our first measurement at the synchrotron was with a sample of x=0.4 value. The result of an uncooled cleavage is shown in figure 7. The features at 43 eV photon energy is a reflection of Te core levels excitated by the second order of the monochromator at the BESSY beamline. In this spectra we also recorded the data of the Hg6s levels (4 to 6 eV). They don't show dispersion.

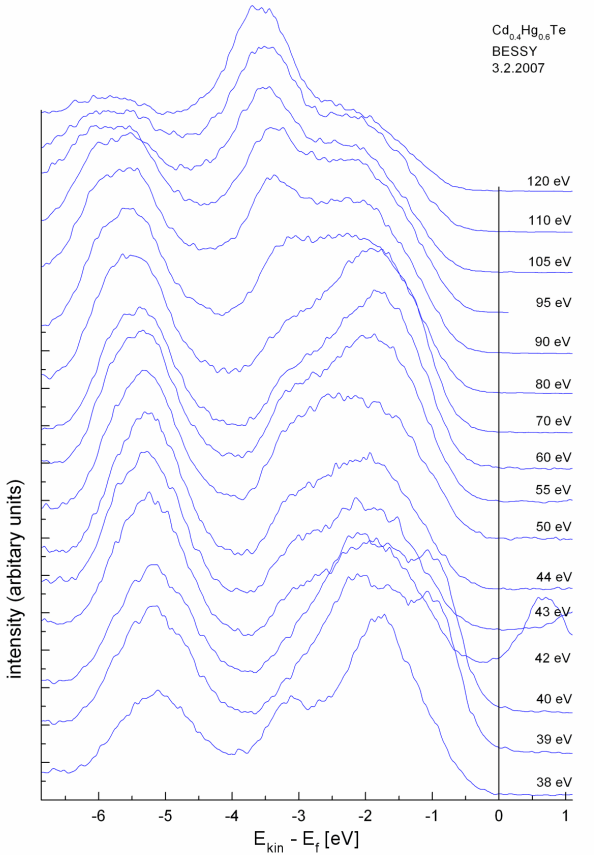

Fig. 7: Dispersion of sample with x=0,4

Although we measured up to 120 eV, no valence band maximum appeared at this energy. The only usable dispersion is seen between 80 and 50 eV and appears to be at 65 eV. Regarding energy and momentum conservation this point belongs to the X point.

In august 2007 at a different beamtime we got a successfull cooled cleavage and observed a dispersion as shown in figure 8 with a sample of x=0.16 value. Based on the experience gathered at the first BESSY beamtime we only measured until 4 eV binding energy. This waterfall spectra shows that the valence band dispers only in this energy range and reaches its maxima (e.g. Γ and VBM) at energies of 120 eV and below 44 eV. Between these energies there is another maxima at approximately 76 eV, it can be seen from 80 to 68 eV. It probably belongs to the X point.

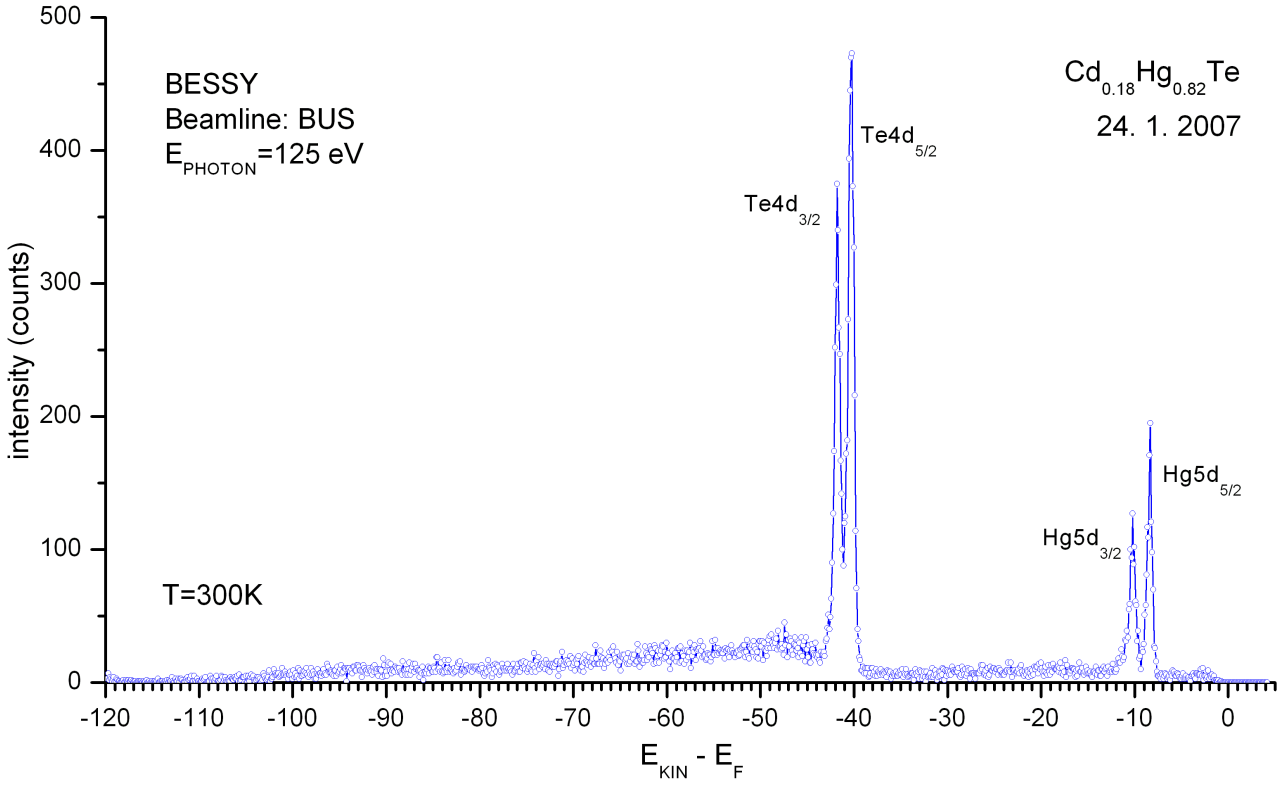

Fig. 6: Overview Photo Electron Spectra of HgCdTe, taken at the BUS beamline at BESSY

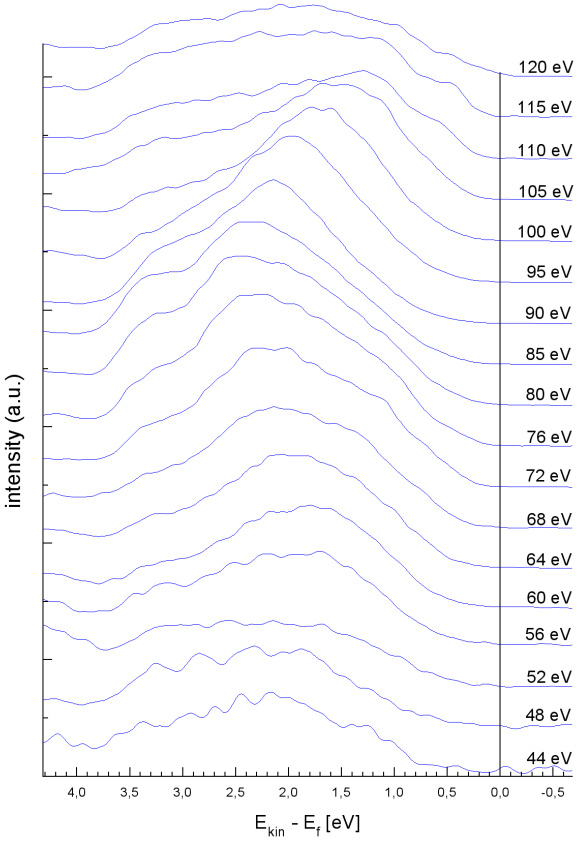

Fig. 8: Dispersion of sample with x=0,163

Our final measurement we did with a sample of x=0.07. In this case we exceeded the photon energy beyond 120 eV to 125 eV, although this was already limited by the beamline and the used grating. But from symmetry conditions it is clear to be seen that the Γ point is located at 120 eV.

In this spectra, though, the X ooint at 65 eV is clear to be seen and shows dispersion from 55 to 75 eV. We took this part also into consideration.

5 Peak fit of the spectra

The next step is to fit peaks into the spectra, according to electronic bands inside the material. We used Gaussian peaks that are folded with the temperature dependant Fermi function. One might expect a Voigt profile instead of a Gaussian fit. The reason is simply a practical one. Using Voigt it was not possible to recieve sufficiant results.

The dispersion near the Γ point at 120 eV has been fitted by several gaussian peaks for each spectra simultanously. The results for x=0.16 are shown in the table 2. Here $h\nu$ is the excitation photon energy at the BESSY Synchrotron Storage Ring, provided by the BUS-Beamline Monochromator.

We assign the Γ_8 band to the volume band V_1 and the Γ_7 band to the volume band V_2. The next fitting results are taken for a x=0.07 sample. Results are shown in table 3

Finally we fited the X-point features of the x=0.4 spectra in figure 7. Results are shown in table 4.

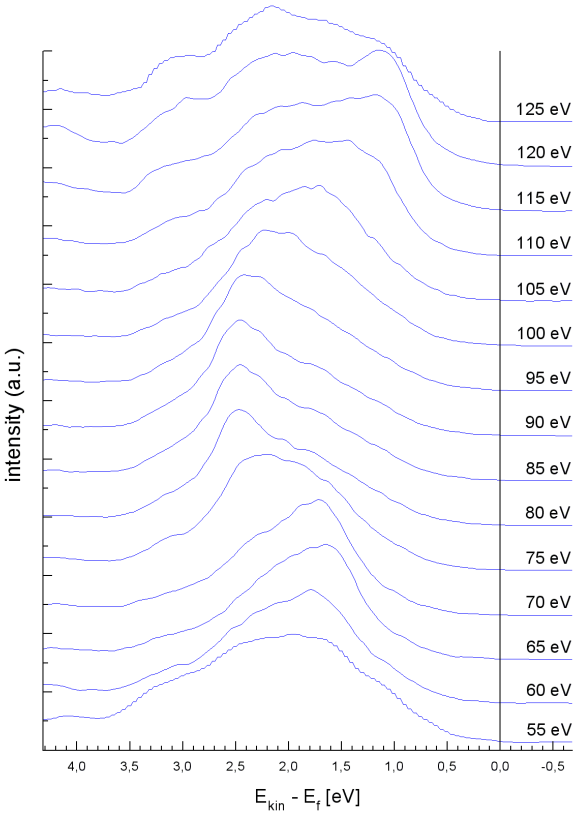

Fig. 9: Dispersion of sample with x=0,07

$h\nu$ eV	V_1 eV	V_2 eV	V_3 eV	V_4 eV	$\lvert\vec{K}\rvert$ Å^{-1}
120	0.413	0.947	1.810	3.226	0
115	0.476	1.046	1.554	2.603	0.0194
110	0.568	1.141	1.302	3.167	0.078
105	0.717	1.115	1.148	3.097	0.175
100	1.531	1.897	2.424	3.078	0.311
95	1.740	1.984	2.366	2.757	0.486

Table 2: Fitting results of spectra in figure 8, x=0.16

$h\nu$ eV	V_1 eV	V_2 eV	V_3 eV	V_4 eV	V_5 eV	$\lvert\vec{K}\rvert$ Å^{-1}
120	1.053	1.605	2.148	2.447	2.910	0.085
115	0.998	1.329	1.864	2.151	3.162	-0.009
110	1.121	1.649		2.248	3.058	-0.094
105	1.513		1.712	2.291	3.029	-0.187
75	1,224	1,674	1,949	2,169	2,375	0.312
70	0,883	1,056	1,708	2,374	2,323	0.161
65	1,111	–	1,005	1,534	1,967	0.005
60	1,09	1,788	2,223	2,524	2,995	-0.157
55	1,389	1,591	1,889	2,356	3,121	-0.326

Table 3: Fitting results of spectra in figure 9, x=0.07

$h\nu$ eV	V_1 eV	V_2 eV	V_3 eV	V_4 eV	$\lvert\vec{K}\rvert$ Å^{-1}
80	1.386	2.017	2.218	2.149	0.457
70	1.282	1.703	2.014	2.710	0.161
60	1.413	1.863	2.753	2.908	-0.157
55	1.335	1.839	2.209	2.726	-0.326
50	0.908	1.529	2.205	2.703	-0.502

Table 4: Fitting results of spectra in figure 7, x=0.4

6 Transfer to K-space

In the previous tables we already assigned a fitting K-value to each photon energy $h\nu$. In first approach we tried to fit the resulting curve with a quadratic expression.

To fullfill momentum conservation as well as energy conservation usually the fittet points are taken into a structure plot to assign each point to a fitting free electron value. In this fitting we add certain primitive lattice vectors to the final state. We already know from former measurements, that most values around 115 eV belong to $\vec{G}_1 = \frac{2\pi}{a}(4,4,0)$ and therefore respecting the Γ point. The dispersion and local valence band maximum around 65 eV belongs to the X point and a lattice vector $\vec{G}_2 = \frac{2\pi}{a}(3,3,1)$. For this prelimary results this is sufficiant. Further details about the structure plot can be found in [19], page 64 to 68.

6.1 Parabolic fit

Commonly in books the law of dispersion for electrons in bulk materials is given by the expression

$$E = E_0 + \frac{\vec{p}^2}{2m_{eff}} = E_0 + \frac{\hbar^2}{2m_e m^*}K^2 \quad . \tag{2}$$

If following we assign the y axsis to the energy in V, measure E_0 also in V and the x values in Å^{-1}. Formula 2 transforms thereby into

$$y = E_0 + \frac{\hbar^2}{2m_e e}\frac{1}{m^*}x^2 = E_0 + \frac{3.806}{m^*}x^2 \quad . \tag{3}$$

We can now use m^* as fit parameter to obtain the results of the next section.

6.2 Nonparabolic fit

According to the Kane model for narrow gap semiconductors the behavior of electrons on top of the valence band is more hyperbolic that quadratic. We fittet our K-values therefore again with the hyperbolic formulae

$$y = E_0 + b\sqrt{\frac{x^2}{m^*} + 1} \quad . \tag{4}$$

The resulting masses differ slightly from the quadradic approximation, as the following section

shows. We have to remind, that the Kane approximation is only valid for energy gaps below 0.35 eV.

7 Results of effective mass

7.1 Dissertation Orlowski: X=0 (HgTe)

First we analyse the reciprocal lattice values N. Orlowski measured in his dissertation [19] on HgTe. In our approach this would represent exactly the x=0 point.

	M_{eff}	ΔE
Γ_8	-1,15	0 eV
Γ_6	-0,49	-0,33 eV
Γ_7	-0,24	-0,92 eV

Table 5: Effective Mass of HgTe.

This data have been directly been digitalisised from figure 10 and been fitted quadratic.

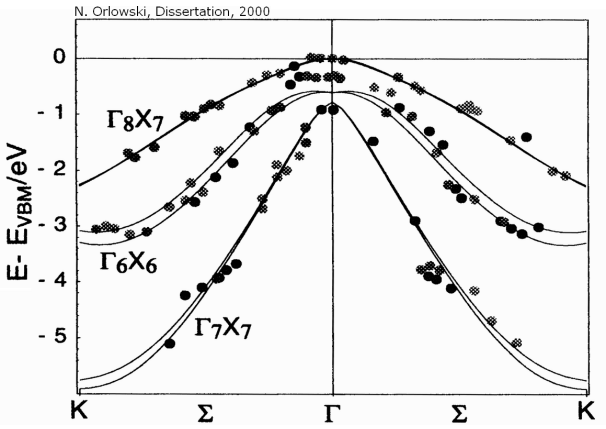

Fig. 10: Bandstructure of HgTe along ΓΣK direction [19].

According to the size of the Brillouin zone the point K here represents a momentum of 1.031 $Å^{-1}$ and defines hereby the x axis.

7.2 $Hg_{1-X}Cd_XTe$: X=0,07 (BESSY, 26.8.07)

In the next approcimation we investigated the data of table 3. Here we have two local maxima of the valence band: one at 115 eV and a second at 65 eV. The first one belongs to the Γ point (Umklappvektor [4,4,0]), the latter one to the X point(Umklappvektor [3,3,1]). The results are shown in table 6

	M_{eff}	ΔE
heavy holes (Γ_8)	0.251	0.977 eV
light holes (Γ_7)	0.097	1.309 eV
heavy holes (X_8)	1.403	1.118 eV
light holes (X_7)	1.267	1.671 eV

Table 6: Effective Mass of $Hg_{0.93}Cd_{0.07}Te$.

The fitting has been done with xmgrace. The measure points and the fitting is shown in figure 11.

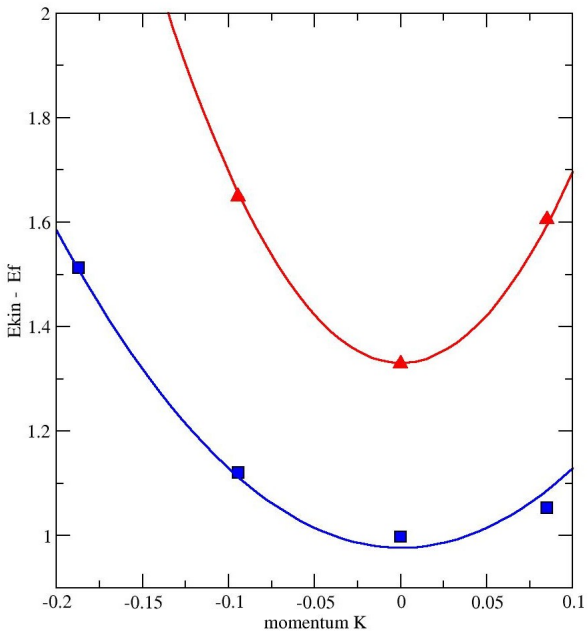

Fig. 11: Dispersion fit in the K space according to the peak positions fitted in table 3.

7.3 $Hg_{1-X}Cd_XTe$: X=0,16 (BESSY, 25.8.07)

In this zero-gap case we were unable to distinguish an additional Γ_6 band, so we could only determine two dispersive bands and two respective effective masses. The fit was done to the data shown in table 2.

	M_{eff}	ΔE
Γ_8	0.55	0,48 eV
Γ_7	0.857	1.08 eV

Table 7: Effective Mass for X=0.163

Surprisingly the mass of the split-off band Γ_7 is heavier than the heavy hole band on the surface of the valence band. The difference in ΔE results in a different investigation of the measured data. Orlowskli *et. al.* used the E_{VBM} as reference and zero where we measured the fermi energy and used this result as zero.

7.4 $Hg_{1-X}Cd_XTe$: X=0,4 (BESSY, 3.2.07)

As already shown in picture 7, the uncooled cleavage of the HgCdTe single crystals lead to undeserved surfaces. In this case we measured not only normal emission but also a superposition of many angles of the surface. Therefore we got to a certain extend energy dependant DoS (Density of States) picture. No valence band maximum can be seen at the expected Γ point. But the X point at 65 eV shows dispersion and we did a fit for comparision with the x=0.07 results.

	M_{eff}	ΔE
X_8	3.994	1.242 eV
X_7	2.259	1.717 eV

Table 9: Effective Mass of $Hg_{0.6}Cd_{0.4}Te$.

X	Te4d$_{5/2}$	Te4d$_{3/2}$	Cd4d$_{5/2}$	Cd4d$_{3/2}$	Hg5d$_{5/2}$	Hg5d$_{3/2}$
0.07	39.873	41.357			7.977	9.807
0.17	39.938	41.416	10.529	11.239	8.025	9.827
0.40	39.968	41.429	10.689	11.398	8.191	9.934

Table 8: Core level positions for Tellurium, Cadmium and Mercury, depending on the composition.

7.5 Dependance of m^* to X value?

Now I can compare the different effective masses m^*_{hh} and m^*_{lh} as well as the energy difference to the split-off band (due to spin-orbit interaction) in dependance of the composition value X. The result for the Γ point is shown in table 10.

X	ΔE_{SO}	m^*_{hh}	m^*_{lh}
0.00	0.92 eV	1.15	0.24
0.07	0.33 eV	0.251	0.097
0.16	0.60 eV	0.55	0.857

Table 10: Effective masses and SO-energy in dependance of X.

Additionally I calculated the respecting values for the X point. The values for X=0 are the same as at the Γ point (see picture 10).

X	ΔE_{SO}	m^*_{hh}	m^*_{lh}
0.00	1.02 eV	1.15	0.24
0.07	0.55 eV	1.40	1.27
0.40	0.48 eV	3.99	2.26

Table 11: Effective masses and SO-energy at the X point.

REMARK: In the advanced laboratory I did the Hall experiment with a sample of $Hg_{1-X}Cd_XTe$ (X=0.203). Our results were a Hall resistivity of $R_H = (772 \pm 8) cm^3/As$ at 77K. For charge carrier concentration (p-type) we got $p = (8.09 \pm 0.08) 10^{15} cm^3$. Deriving the arising of the values with temperature and performing a linear approximation we got to values for [Anstieg]. Comparison of coefficients resultet in

$$E_g = 2ka \tag{5}$$

and therefore in the following energy gap results:
$E_g = (0.0960 \pm 0.0009) eV$ from conductivity
$E_g = (0.1143 \pm 0.0001) eV$ from Hall coefficiant.

The mobility of holes was $\mu = (390 \pm 9) \frac{cm^2}{Vs}$. The impulse relaxation time $\tau = m^* \mu / e$ resulted in $\tau = m^* (2.22 \pm 0.05) 10^{-13} s$. Finally the mobility ratio was $b = \frac{\mu_n}{\mu_p} = (45 \pm 1)$.

8 Core Level Shift

In former UPS studies of HgCdTe Shih *et. al.* reported a core level shift for the Hg5d and Cd4d bands [10]. With the photon energy at BESSY avaliable we checked the core levels of Te4d as well. Our results for different compositions are shown in table 8.

Interestingly the spin-orbit split energy of Te and Hg changes with the composition, while the Cd value remains almost constant. As can be seen in table 12 for Te the difference reaches $\Delta_{Te} = 23meV$ and for Hg $\Delta_{Hg} = 87meV$.

X	Te4d	Cd4d	Hg5d
0.07	1.484		1.830
0.17	1.478	0.710	1.802
0.40	1.461	0.709	1.743

Table 12: Spin orbit split energy, depending on x.

The relative positions shift too. From table 13 we see a shift of up to $\Delta_{Te-Cd} = 146meV$ for Cadmium and Tellurium, where the shift between the core levels of Tellurium and Mercury values up to $\Delta_{Te-Cd} = 136meV$.

X	Te-Cd	Te-Cd	Te-Hg	Te-Hg
0.07			31.896	31.550
0.17	29.409	30.177	31.913	31.589
0.40	29.279	30.031	31.777	31.495

Table 13: Relatice energy positions of core levels.

In the work of Silberman *et. al.* [7] they measured values for the Hg5d core levels at 7.8 eV and 9.5 eV. The values for Cd4d were 10 eV and 10.7 eV. Depending on the composition Shih [10] reported a shift of 0.1 eV for Hg core levels and 0.25 eV for Cd core levels, respectively.

9 Conclusion

As we've seen the ARPES method is a powerful tool to determine the electronical bandstructure of a given material. Because of its momentum resolving possibilities we have direct access to the dispesion of the valence bands inside the crystal.

Our results also show, how filigrant this method is to a good prepared surface. Therefore it is nessesary to check the surface quality as well as the single crystal quality using other methods. As for HgCdTe bulk crystals, that are not grown inside the vacuum, a clean UHV surface can only be achieved by cooled cleavage.

The effective mass for the heavy holes should be in the regime of $0.45 < m^* < 0.55$ in a nonparabolic approximation. In some cases we got similar results by ARPES, while in other cases these values differ about more than 50 % . This may be to the different ways these values are derived. For composition values $0 < X < 0.6$ the mass of light holes should symetric and in between 0.02 and 0.05 in a temperature range from 77 to 300 Kelvin.

For x=0.07 we got a value even lower than that with our result $m^* = 0.097$ (see table 10).

References

[1] H. Hertz. Über den Einfluss des ultravioletten Lichtes auf die elektrische Entladung. *Ann. Phys.* **31**, 983 (1887).

[2] W. D. Lawson, S. Nielson, E. H. Putley, and A. S. Young. Preparation and properties of HgTe and mixed crystals of HgTe-CdTe. *J. Phys. Chem. Solids* **9**, 325-329 (1959).

[3] D. Long and J. L. Schmit. Mercury-cadmium telluride and closely related alloys. *Semiconductors and Semimetals*, Vol. 5, pp. 175-255, edited by R. K. Willardson and A. C. Beer, Academic Press, New York (1970).

[4] D. A. Shirley. High-Resolution X-Ray Photoemission Spectrum of the Valence Bands of Gold. *Phys. Rev. **B*** 5, 4709-4714 (1972).

[5] G. L. Hansen, J. L. Schmit, and T. N. Casselman. Energy gap versus alloy composition and temperature in $Hg_{1-X}Cd_XTe$. *J. Appl. Phys.* **53**, 7099-7101 (1982).

[6] P. Morgen, J. Silberman, I. Landau, W. E. Spicer, J. A. Wilson. Stability of an atomically clean $Hg_{1-X}Cd_XTe$ surface in vacuum and under O_2 exposure. *Journal of Crystal Growth* 56, 493-497 (1982).

[7] J. A. Silberman, P. Morgen, I. Lindau, and W. E. Spicer. UPS study of the electronic structure of $Hg_{1-X}Cd_XTe$: Breakdown of the virtual crystal approximation. *J. Vac. Sci. Technol.*, 21(1) pp. 142-145 (1982).

[8] W. E. Spicer, J. A. Silberman, and I. Lindau. Band gap variation and lattice, surface, and interface "instabilities" in $Hg_{1-X}Cd_XTe$ and related compounds. *J. Vac. Sci. Technol. A* 1(3) pp. 1735-1743 (1983).

[9] S. Tougaard. Deconvolution of loss features from electron spectra. *Surface Science* 139 (1984) pp. 208-218.

[10] C. K. Shih and W. E. Spicer. Photoemission studies of core level shifts in HgCdTe, CdMnTe, and HgZnTe. *J. Vac. Sci. Technol. A*, 5(5) pp. 3031-3034 (1987).

[11] C. K. Shih, J. A. Silberman, A. K. Wahi, G. P. Carey, I. Lindau, and W. E. Spicer. Angle resolved photoemission study of the alloy scattering effect in $Hg_{1-X}Cd_XTe$. *J. Vac. Sci. Technol. A*, 5(5) pp. 3026-3030 (1987).

[12] M. A. Berding, A. Sher, A-B Chen and R. Patrick. Vacancies and surface segregation in HgCdTe and HgZnTe. *Semicond. Sci. Technol.* vol. **5** pp. S86-S89 (1990).

[13] A-B Chen, Y-M Lai-Hsu, S. Krishnamurthy, M. A. Berding, and A. Sher. Band structures of HgCdTe and HgZnTe alloys and superlattices. *Semicond. Sci. Technol.* vol. **5** pp. S100-S102 (1990). doi:10.1088/0268-1242/5/3S/021

[14] W. M. Higgins, G. N. Pultz, R. G. Roy, R. A. Lancaster, J. L. Schmit. Standard relationships in the properties of $Hg_{1-X}Cd_XTe$. *Vakuum Science and Technology* **A** 7 (1989), p 271-275.

[15] G. Lévêque, B. Orsal, R. Alabedra, J. C. Flachet. Valence band structure of $Cd_{0.7}Hg_{0.3}Te$ determined by angular resolved photoemission. *Journal of Crystal Growth* 101, p 364-367, (1990).

[16] T. Plake. Aufbau und Inbetriebnahme des Photoemissionsexperimentes HIRE-PES: Charakterisierung und erste Untersuchungen an $Bi_2Sr_2CuO_6$-Hochtemperatursupraleitern. *Diplomarbeit*, AG EES, (1998).

[17] N. Orlowski, J. Augustin, Z. Golacki, C. Janowitz, R. Manzke. Direct evidence for the inverted band structure of HgTe. *Phys. Rev. B, Rapid Communications*, 61, R5058-R5061, (2000).

[18] B. H. Koo, Y. Ishikawa, J.F. Wang, M. Isshiki. Crowth of $Hg_{1-x}(Cd_{1-y}Zn_y)_xTe$ epilayers on (100) $Cd_{1-y}Zn_yTe$/GaAs substrates by ISOVPE. *Materials Science and Engineering*, B66, 70-74, (1999).

[19] N. Orlowski. Untersuchung der elektronischen Struktur von HgSe und HgTe mittels winkelaufgelöster Photoemission. *Diplomarbeit*, AG EES, (2000).

[20] C. Janowitz, N. Orlowski, R. Manzke, Z. Golacki. On the band structure of HgTe and HgSe - view from photoemission. *Journal of Alloys and Compounds*, 328, 84-89, (2001).

[21] W. E. Bies, H. Ehrenreich, and E. Runge. The Thermal Conductivity Reduction in HgTe/CdTe Superlattices. arXiv:cond-matter/0112039v1.

[22] P. Norton. HgCdTe infrared detectors. *Opto-Electronics Review* **10**(3), 159-174 (2002).

[23] Yue Wang, Quanbao Li, Qinglin Han, Qinghua Ma, Rongbin Ji, Bingwen Song, Wanqi Jie, Yaohe Zhou, Yuko Inatomi. Growth and properties of 40mm diameter $Hg_{1-X}Cd_XTe$ using the two-stage Pressurized Bridgman method. *Journal of Crystal Growth* 263 (2004) 54-62.

[24] Derek Ives, Nagajara Bezawada. Large area near infra-red detectors for astronomy. *Nuclear Instruments and Methods in Physics Research* **A** 573 (2007) 107-110.